THESIS

EXTENDING THE LIFE OF ELECTROCHEMICALLY DEPOSITED ANODES IN 3D SODIUM ION BATTERIES WITH CPAN

Submitted by

Dylan Media

Department of Chemistry

In partial fulfillment of the requirements

For the Degree of Master of Science

Colorado State University

Fort Collins, Colorado

Spring 2025

Master's Committee:

Advisor: Amy Prieto

Anthony Rappe
Reza Nazemi

ABSTRACT

EXTENDING THE LIFE OF ELECTROCHEMICALLY DEPOSITED ANODES IN 3D SODIUM ION BATTERIES WITH CPAN

Humanity constantly seeks to improve the simplicity of their lives, and as such develops technologies to assist with this endeavor. Almost all of these technologies rely on electricity. From large stationary objects to the small mobile devices we see everywhere, they must be charged. For some this means operation almost exclusively on a battery, for others they rely on constant power from the power grid, and most use a rechargeable battery charged from the power grid as a blend. But even power stations have limits for how much they can generate at a time and need to rely on power generated during low demand times to supplement higher demands, and such the power grid also relies on batteries. Chapter I discusses the basis of why energy storage is so important, the history of the modern lithium-ion battery, and where storage technology is heading to improve supplemental battery types. The basics of why sodium ion batteries are attractive as a supplement to lithium-ion batters is outlined. Finally, the geometries of 3D batteries are described, and a key feature leading to uneven distribution of material on 3D electrodes is highlighted.

Chapter II focuses on developing a procedure to cyclize polyacrylonitrile (PAN) to act as a binder to keep material in electrical contact to the anode current collector after it fractures and separates. Simple equipment such as a dip coater and a tube furnace are used to evenly coat the substrate with the precursor, which is then annealed to form cPAN. Verification of the cyclization of PAN to form cPAN is done via Fourier Transform Infrared (FTIR) analysis, and sample

thickness is measured using scanning electron microscopy (SEM). Once the procedure for the fabrication steps is verified, the actual anodes must be made. In chapter III, cyclic voltammetry is used to get the correct parameters for sample electrodeposition and the anodes are made. After samples were annealed with a layer of cPAN, SEM and energy-dispersive X-ray spectroscopy (EDS) are used to characterize the samples. There is a detailed discussion for the fabrication of a pouch half-cell, and some trends observed when they are evaluated as an electrode using battery cycler.

Chapter IV attempts to get a realistic application by placing cPAN coated anodes in a full cell and placing them on a battery cycler. Every step along the way was characterized by measuring the internal resistance, which is noted as an indicator of how or why the cells may be acting abnormally. In conclusion, the overlap of each section is summarized and discussed. The hypothesis for why the cells do not cycle effectively is that the polymer is too thick. Future work will focus on repeating the coating of cPAN onto antimony anodes but with better control over thickness. Refinements to the process such as a thinner polymer layer, calendaring, and a better contact and compression system could provide insight and useful results in the future.

TABLE OF CONTENTS

Chapter 1- Exploring Next Generation Batteries: Sodium Ion Battery Chemistry and 3D Architectures.

1.1 The Growing Need for Energy Storage

As our world moves forward, we find ourselves developing new technologies to enable better quality of life in every aspect: food, communications, entertainment, and health. If we just focus on entertainment as an example, applications are widely varied from our stationary computers and televisions to mobile devices such as laptops, phones and children's toys. The proliferation of such devices has significant implications. All of these technologies are powered by electricity, and thus must have a source for that electricity. Because many of these devices are mobile, that electricity must be stored in a battery in the device.

Many corded technologies used in our day to day are simply plugged into an outlet and that power comes from the power grid. Most of this power is generated and used immediately from the many variations power plants we have around the country. The general living habits of most countries results in that demand being around the same time daily for most populations. Spikes in the morning as everyone is waking up, and in the evening as the population is off work and living their individual lives, turning on the stationary objects or charging the mobile ones[1]. This is often the cause of blackouts in very large cities where power demand surges exceed the power grid's ability to supply it. "Green" options such as solar and wind, are becoming more prevalent, but peaks in generation aren't consistent and are shifted in time relative to demand peaks. Solar panels can supplement the energy fed into the grid from power stations, but the sun is brightest in the middle of the day, so the electricity peaks midday when demands are low and can vary greatly day

to day and year-round[2]. Wind power can supplement the grid as well but this is also not as consistent and reliable everywhere[3]. This means that strengthening city power grids, especially those making use of renewable technologies, must utilize large scale batteries for mass energy storage banks to store the excess generated when at high production/low utilization times.

This balance of where and when we can generate power emphasizes why both small, light, and mobile batteries and large, dense, and stationary batteries must be made. Batteries can fall into two categories, primary or secondary. Primary batteries are non-rechargeable and are great for low power demand applications. These batteries last a very long time and fit in with simple devices that themselves may last quite a while but have short intended-use windows, such as simple children's toys. To keep these straightforward and easy to produce, primary batteries are non-rechargeable, generating waste. As our demand for technology is increasing, and the power demand for our batteries keeps growing, replacing the batteries in everything frequently would get very time-consuming and require a lot of resources. So secondary batteries fill this role, being similar but rechargeable. However, to make this possible we must use different materials in the battery so that it can survive frequent charge and discharge cycles. Because these batteries are rechargeable, their degradation mechanisms are very different. A main degradation mechanism that will be discussed in this thesis is the change in volume as the anode shrinks and swells during charging and discharging operations.

1.2 Response to the Energy Storage Demands.

1.2.1 Supplementing Lithium-Ion Batteries with Sodium Ion Batteries

Currently lithium-ion batteries (LIBs) dominate the market, and the demand is only going up. Lithium, as one of the smallest elements, serves as an incredibly attractive choice to act as the primary charge carrier in batteries. This element is small, light, very electropositive, and has a large potential difference between the neutral an +1 cation. This results in lithium having a very negative reduction potential, allowing it to have large voltage window when part of the cathode against a variety of anodes. Lithium is often able to be stored by intercalation because of its size, such as with its most common anode, graphite, providing a high energy density. Intercalation electrodes don't change volume significantly when charged. However, a conversion electrode, where the anode changes its structure to incorporate the lithium ion, can provide much higher energy density but this volume change is very large, resulting in the previously mentioned shrinking and swelling that can cause pulverization over time.

However, global stores of lithium are limited and costs are increasing as supply chains are challenged, especially as geopolitical tensions are stressed[4]. This drives prices of lithium up and makes battery products more expensive. Despite the small size LIBs, high energy density hurt their charge and discharge rates long term. This makes LIBs less favorable for large scale energy storage. To provide an alternative, research in sodium-ion batteries (SIBs) are pushing to make an energy storage device that is cheaper and safer

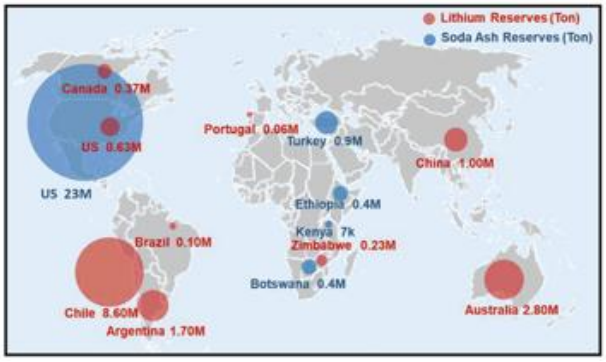

Figure 1-1: Global distribution of Sodium ash reserves in blue and Lithium reserves in red. Figure taken from Hirsh et al. Figure 1.

to help fill the demand. Figure 1-1 shows the global distribution of lithium and sodium reserves in tons[4]. While this is of specific material reserves, recovery of these elements is possible through other means, the process of this recovery just isn't as cost effect as mining the reserves yet, though in time and the ocean itself serving as a type of sodium reserve it will likely be the cheapest recovery option. By adding a potential competitive technology, the situation would then be that not every battery must be a LIB and demand can be reduced. Moreover, SIBS at lower energies tend to have less safety issues and are less prone to thermal runaway.

With the differences in material properties sodium is not being called on as a direct replacement for lithium, but a means to augment energy storage alongside LIBs when possible. As discussed previously different situations will call for different types of batteries. Figure 1-2 shows a distribution of types of batteries and what characteristics should indicate what they may best be used for with our current technologies[4,5].

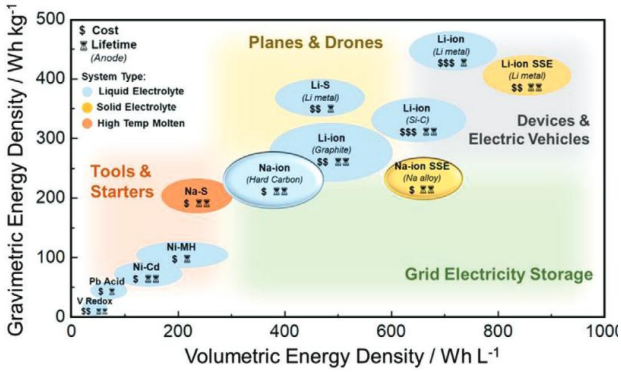

Figure 1-2: Volumetric Energy Density vs Gravimetric Energy density with highlighted regions for systems in which that ratio is best suited. Figure taken from Hirsh et al. Figure 1

1.2.2. Introduction to 3D Batteries.

The biggest issue with the conversion to sodium batteries is power density and life cycle. Because of the power density lag of SIBs, they just aren't as appealing for high-power energy demands. With the shorter life cycles, we still come back to the inconvenience of replacing the battery at more frequent intervals. While graphene can work well as an intercalation anode with lithium, it struggles to maintain any capacity of sodium. For most anode materials to incorporate the larger sodium ion, they tend to be the previously mentioned conversion anodes. One of the

most energy dense anodes for sodium is antimony, because it can incorporate three sodium ions for each antimony. However, this conversion results in a 293% expansion in volume. This will accelerate the mechanical pulverization of the material.

To increase power density, the active material needs to be thin (for short diffusion paths) but at a high areal loading. Because electrochemistry requires contact on the current collector, surface

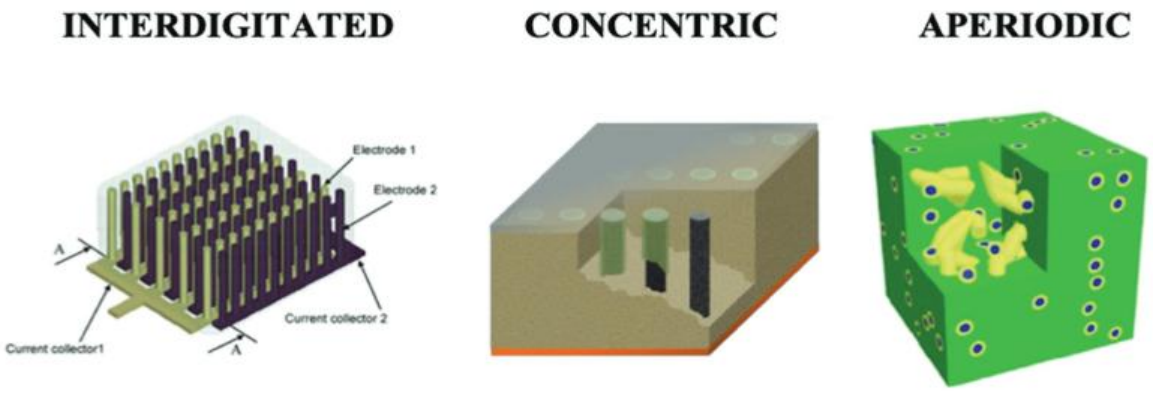

Figure 1-3: Typical geometries for 3D batteries. Interdigitated (right): columns of each electrode are near each other with gaps of electrolyte. Concentric (center): columns of anode (black)are extended and insert into holes in the cathode (tan) with small tolerances to prevent shorting and allow electrolyte. Aperiodic (left): metal weblike structure (blue) is used as a current collector coated in anode(yellow), typically some form of polymer or solid electrolyte separates anode from filled cathode (green). Taken from Long et al figure1

area per footprint is a key feature when this is being developed. To this end, development of 3D batteries is becoming a focus of research. As opposed to 2 flat surfaces facing each other, 3D batteries are a system in which the anode, cathode, and electrolyte can interact with each other in more than one dimension, resulting in less bulk inaccessible material and greater surface area in the same original volume. However, the drawback to this is that these surfaces then require more bends and changes in shape. This will result in inconsistent layers of active material on both surfaces and inherent structural weak points for early failure. Figure 1-3 shows common geometries of 3D batteries[6].

Figure 1-4 shows the geometry and structure of the aperiodic foam used in this experiment. The blue arrow pointed at the bulbus end of where the struts turn will be referred to as points throughout this thesis. When depositing material these being more exposed will concentrate lines of flux and result in more deposited material in these regions. The yellow arrows direct attention to valleys, areas that dip between points. Valleys are low flatter areas which experience lower flux during deposition, which results in less material in these regions. With more material on the curving outward points and less material on the curving inward valleys, we can see where ideal weak points exist for fracturing to occur.

1.3 Thesis Focus and Chapter Overviews

1.3.1 Intent of experimentation.

The focus point of this thesis was built around these ideas, and the next step associated with some attempts found in literature to extend lifetime by providing structural support. To do this, two projects, from Kelly Nieto and Dan Windsor, senior members of our lab, were blended. First Dr. Windsor was testing strengthening options by coating a 2D substrate with polyacrylonitrile (PAN) and annealing it to cyclize the polymer[7]. This was intended to extend battery life by keeping fractured material in electrical contact so that the capacity of the material was not lost to the cell. Second Dr. Nieto's work explored an antimony anode on a 2D substrate and transitioning that to a 3D cell[8]. From there

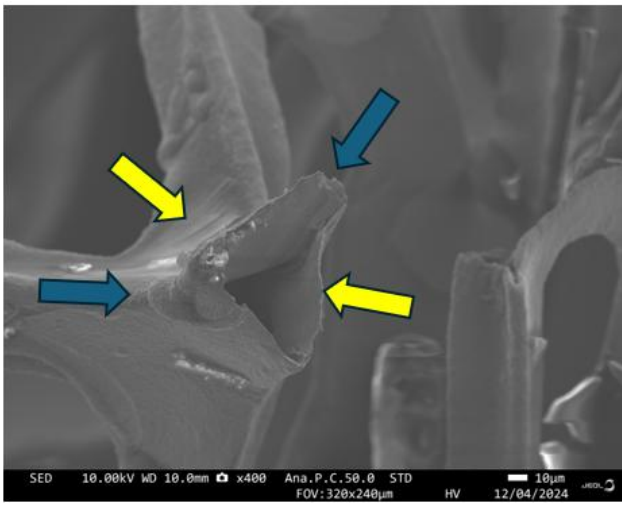

Figure 1-4: SEM image of the aperiodic substrate used throughout this experiment. Blue arrows are used to assist identifying regions referred to as points, yellow areas to help identify regions referred to as valleys.

she was able to get an anode half-cell operation using antimony electrodeposited onto an aperiodic 3D substrate with sodium. Over the course of dissertation, we sought to transition Dr. Windsors 2D work to a 3D anode like that Dr. Nieto had success with.

1.3.2 Chapter Overviews

1.3.2.1 Chapter 2- Verifying cPAN Formation and Desired Procedure

Dr. Windsor's primary method of coating PAN was by drop casting and spinning the substrate. This approach works well on a 2D plane and when the sample is round. For this experiment the method was shifted to mechanically dip coating each of the substrates at various intervals to get even coating of the polymer onto a foam electrode. A tube furnace was used to cyclize the PAN into cPAN. Following the polymer annealing the samples were then characterized to verify that the PAN did in form the cyclized chains intended. FTIR and SEM are utilized for data analysis.

1.3.2.2 Chapter 3- Fabrication of Pouch Half-Cells for cPANs Effects on an Anode

In this chapter antimony is electrodeposited on nickel foam, in similar concentrations to that in which Dr. Nieto used. Samples are left uncoated as the control, and some are coated with cPAN to try to improve battery lifetime. A detailed description of a pouch cell is given. SEM and EDS are used to observe patterns of deposition with the coating. Issues with resistance and EIS are discussed. A first look at cPAN coated anode cycling data is recorded.

1.3.2.3 Chapter 4- cPAN Anodes in Full Cells and Conclusions.

Full cells are assembled to get a picture of how cPAN can impact the cell. An additional discussion is focused on developing hypotheses to explain why the electrodes in this thesis resulted in high internal resistances, and an analysis of the full data set is given. The chapter and thesis are rounded out with the next steps and improvements to be made for the future.

1.4 References

(1) Torriti, J. Understanding the Timing of Energy Demand through Time Use Data: Time of the Day Dependence of Social Practices. *Energy Res. Soc. Sci.* **2017**, *25*, 37–47. https://doi.org/10.1016/j.erss.2016.12.004.

(2) *How much electricity do solar panels produce?*. National Energy Action (NEA). https://www.nea.org.uk/who-we-are/innovation-technical-evaluation/solarpv/how-much-electricity-solar-produce/ (accessed 2025-03-18).

(3) *How much US electricity comes from wind power?*. USAFacts. https://usafacts.org/articles/how-much-us-electricity-comes-from-wind-power/ (accessed 2025-03-18).

(4) Hirsh, H. S.; Li, Y.; Tan, D. H. S.; Zhang, M.; Zhao, E.; Meng, Y. S. Sodium-Ion Batteries Paving the Way for Grid Energy Storage. *Adv. Energy Mater.* **2020**, *10* (32), 2001274. https://doi.org/10.1002/aenm.202001274.

(5) Zhao, L.; Zhang, T.; Li, W.; Li, T.; Zhang, L.; Zhang, X.; Wang, Z. Engineering of Sodium-Ion Batteries: Opportunities and Challenges. *Engineering* **2023**, *24*, 172–183. https://doi.org/10.1016/j.eng.2021.08.032.

(6) Long, J. W.; Dunn, B.; Rolison, D. R.; White, H. S. 3D Architectures for Batteries and Electrodes. *Adv. Energy Mater.* **2020**, *10* (46), 2002457. https://doi.org/10.1002/aenm.202002457.

(7) Windsor, D. S.; Perez, M. J.; Snyder, E. R.; Neisius, N. A.; Otten, R. A.; Hall, S. C.; Tibbetts, C. A.; Krummel, A. T.; Prieto, A. L. Multifunctional Cyclized Polyacrylonitrile (cPAN) as a Coating for Sb-Based Anodes in Sodium-Ion Batteries. *ACS Appl. Mater. Interfaces* **2025**, *17* (1), 2117–2129. https://doi.org/10.1021/acsami.4c13887.

(8) Nieto, K. Tuning Antimony Anodes Through Electrodeposition to Inform on the Reaction and Degradation Mechanisms in Sodium Ion Batteries, Ph.D. Dissertation, Colorado State University, 2023.

Chapter 2- Verifying cPAN Formation and Desired Procedure

2.1 Background

As a sodium-ion battery charges the anode material swells immensely as it integrates the sodium, then shrinks back down as the sodium moves back to the cathode (during discharge). In the particular example discussed in this thesis, the crystalline antimony can accommodate 3 sodium ions when fully charged to form Na_3Sb, resulting in a 293% volume expansion[1]. This change in size causes fractures in the material and over time these fractures propagate with repetition, resulting in mechanical pulverization. This causes parts of the material to lose contact with the substrate acting as a current collector, and subsequently the loss of its mass for useful capacity retention. To help alleviate this degradation mechanism, battery scientists have been trying to include additional components to help keep the material in contact with the substrate. One area of active research is to use electrically conductive polymer binders. The purpose of using a polymer binder is so that when the active material fractures the binder helps keep the material in contact with the current collector. However, over time expansion and contraction can lead to damage to the polymer and causing continuity failure, and that material is still lost. The advantage to using a polymer that is conductive, damage will still occur but the reduction of the capacity lost is reduced as there is still a path for electron movement to substrate. That means that material will still be useful even after separating from the current collector and the batteries life should be extended.

A conductive polymer that has been of significant interest in the literature, especially for 2D and all solid-state batteries, is cyclized polyacrylonitrile (cPAN)[2–4]. PANs basic structure, (a) in Figure 2-1, shows that there is little flexibility in electron density with the triple bonded C-N

resulting in a more resistive and polymer. However, at higher temperatures, around 250-300 °C[2], the molecule can rearrange (cyclize) and create rings with a single and double bond to the nitrogen. This delocalization allows a significant amount of electron mobility and movement within the rings and, to an extent, the full molecule, and the strength of the nitrile groups should limit the ring chain groups to 3-5[2], such as (b) in Figure 2-1. Longer chains must then break up the rings every so often as shown in (c) of Figure 2-1, allowing the required flexibility of a polymer to stretch and bend as desired with the material. If heated and cyclized at higher temperatures cPAN will form graphite-like sheets, which increases the conductivity and strength of the polymer but also the rigidity of it[1,4] and should be identifiable based on a lack of hydrogen in the structure.

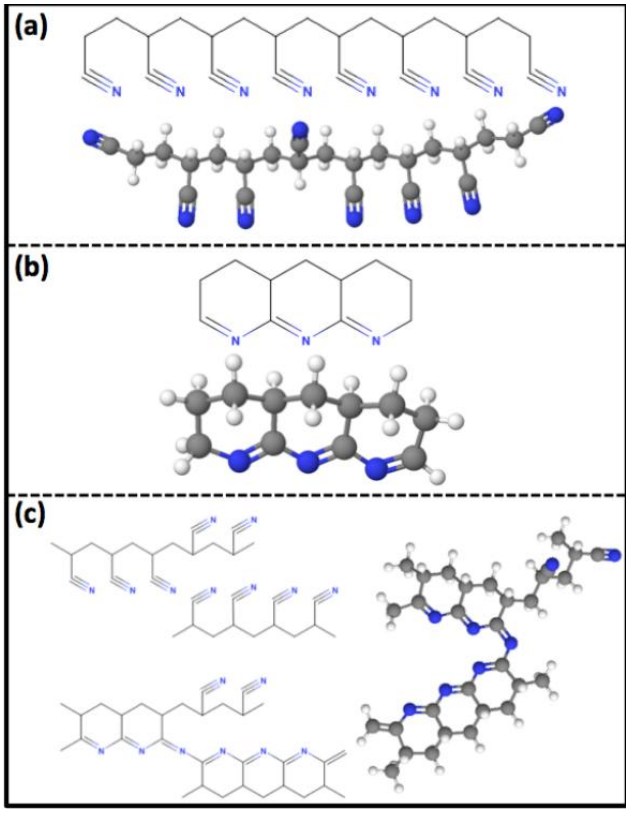

Figure 2-1: Variations of polyacrylonitrile (PAN). (a) simple polymer chain. (b) cyclized 3 polymer chain. (c) extended polymer chain with multiple cyclized series. Lee- Figure 2, page 4.

To start independent research, it was necessary to verify the process to form cPAN was working properly as it was going to be done frequently, and the verification can damage the material. So, ensuring the method worked properly should save time, as it just wouldn't be possible to check each sample. Additionally, the concentration of the solution used to coat the substrate as well as the number of times the substrate was dipped should affect the thickness of the polymer.

So, while verifying the cycling procedure worked correctly, variations in concentration and number of dips were also done to try to make a cPAN coating that was resilient to fracturing from the size fluctuation of the material below it.

2.2 Experimental

2.2.1 Determination of Preferred Concentration of PAN for Dip Coating.

To determine the preferred concentration for coating and then the number of dips, we started with a 1L batch of 1M PAN that was prepared for use as a 1M solution or in any series of required dilutions. For this the molar mass of the monomer of PAN was used to determine total mass to use for the 1M PAN(Sigma-Aldrich) was dissolved in 1 L of dimethylformamide (DMF) (Fischer Chemical). All substrates were cut from a nickel foam roll (MTI, 1.25 cm thick) to an approximately 4 cm by 1 cm strip.

The first 3 solutions were prepared consisting of 1M, 0.5M, and 0.25M concentrations of PAN. Using a Progressive Automations Dip Coater, 6 of the nickel foam strips were dipped individually 10 times, being held in solution for 5 seconds and then removed and allowed to rest out of solution for 10 seconds. To have 2 strips in each of the solutions they were placed side by side to be simultaneously coated. The movement speed of 500 mm per minute allows the solution to slowly fill in between the tendrils of the substrate during dipping. These substrates were then allowed to dry in a vacuum desiccator overnight at room temperature.

The samples were annealed to cyclize the PAN in a Lindburg Tube Furnace. The sample were placed in the center position of the furnace (where the thermocouple is) and the chamber was purged of air by drawing a -0.7 MPa vacuum utilizing a vacuum pump and returning to atmospheric pressure under pure argon three times, then maintaining a vacuum with a 100 cc/min argon flow

rate for a minimum of 30 minutes. The furnace was then raised to 300 °C at a rate of 10 °C/min and held there for 4 hours. Once that time was up the furnace heating element, vacuum pump, and argon flow were all turned off and allowed to cool inside the furnace until 100 °C. At this time the hood for the furnace and tube were opened to break vacuum and remove the samples. The samples were allowed to passively cool in the ceramic boat for an additional hour before being returned to the vacuum desiccator until needed for analysis. These samples were analyzed using Fourier-Transform infrared spectroscopy (FTIR) taken on a ThermoScientific Nicolete Summit FTIR Spectrometer to confirm cPAN formation. They were then flash frozen by immersing in liquid nitrogen for 30 minutes and cut in half horizontally at the midpoint as seen in Figure 2-2 to be observed using a JEOL JSM-IT800 scanning electron microscope (SEM).

2.2.2 Varying the number of dips.

In the second round of the experiments the 1M solution was chosen, the choice of this concentration will be discussed later. The 3 substrates were dipped in fresh solutions, under the same conditions but varying now the number of dips: 25, 50, and finally 100 times. These too were then allowed to dry overnight in the vacuum desiccator prior to annealing using the same method. Follow up analysis was done in a similar method as before; however, the samples were cut vertically, see Figure 2-2.

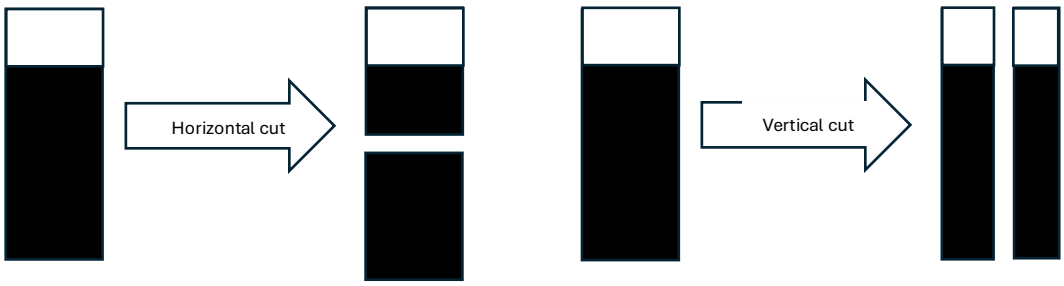

Figure 2-2: demonstrations for where cuts were made to the anodes. Left-Horizontally. Right- Vertically.

2.3 Discussion and Results

2.3.1 Confirming cPAN with FTIR

During the first round of FTIR verification of the materials a background spectrum of the bottom of the analysis surface plate was taken as a control, since the material was a foam and signal from the analysis was assumed to be most likely to see the plate as well. However, additional errors came from the exposed nickel oxides and the varying shapes of the foam structure. So, an additional verification of just the nickel foam was analyzed. Above, Figure 2-3 contains the FTIR traces of each of the samples and the nickel foam. This was compared to assigned cPAN peaks in literature[3,4]. When looking at the bare nickel trace there is a noise anomaly around 2200-1800 wavenumbers which we should see in the in all other samples, this area could also have a weak signal that would indicate a C≡N bond that we would expect in unreacted PAN. We can also see noticeable peaks around 1600 relating to C-C or C=N bonds or potentially aromatic rings[6]. Slightly to the left sits a peak at 1370 wavenumbers which has been indicative of the C-H bonds indicating

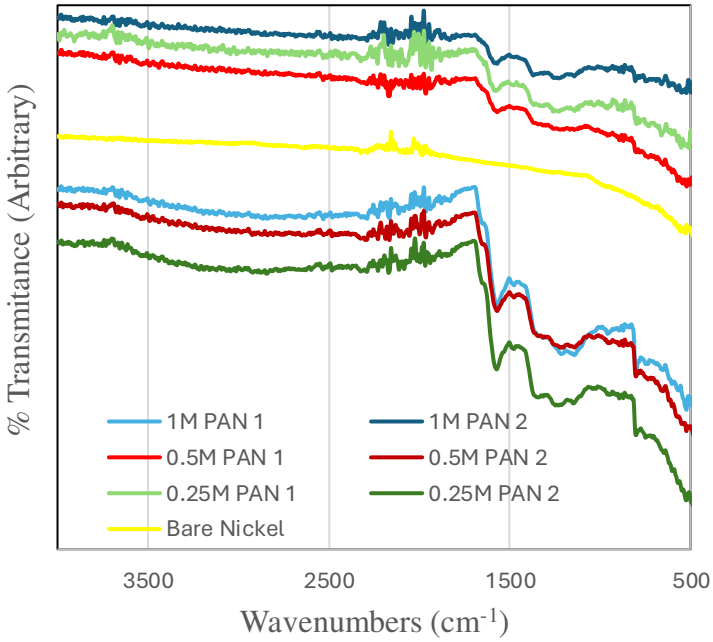

Figure 2-3: FTIR plots of first 6 samples made. First substrates dipped for that solution type is in the lighter hue of the concentration color with the second being darker. The 1M PAN solution is tracked in blue. The 0.5M PAN is in red. The 0.25M PAN is in green. The % transmission has been shifted to emphasis the similarity in patterns. The bare nickel trace to compare the distortion due to the 3D texture is in yellow and shifted between the two patterns for reference.

that we haven't over heated[5]. At about 800 wavenumbers there is a peak indicated by a cliff with a drastic drop which can be related to C-N-C bonds[6]. This peak may be difficult to see due to the gradual drop caused by the uneven texture of the substrates. A later verification of non-cyclized PAN showed the absence of the 2240 peak as well as the presence of the 1600 and 1370 peaks. However, it has a definitive 1100 wavenumbers peak and absence of 800 wavenumber peak. So, using these peaks, it can confidently be stated that cPAN was formed from all 3 concentrations.

All 6 substrates were annealed at the same time side by side to their pair concentration in the ceramic boat, this caused one to be flat along the bottom and one to be slightly angled on its side with one edge on the bottom and one edge on the side demonstrated in Figure 2-4. When looking at the patterns, there was a clear distinction between the samples where half formed a simple curve with simple peaks were expected and a second set that was simply more intense. When plotting the data the ones dipped first in the set of were identified by one and the second identified as two. It was assumed that all 6 should anneal the same, this clearly wasn't the case. Upon further investigation the difference in these was if the flat on the bottom of the boat or slightly on its edge. In both instances we can determine that PAN is being cyclized as desired. If one or the other would be more desirable was not considered at the time and wasn't revisited. For consistency, the maximum number of samples to be annealed at a time was limited to 3 so that they could all be flat on the bottom and centered to the sides in the ceramic boat.

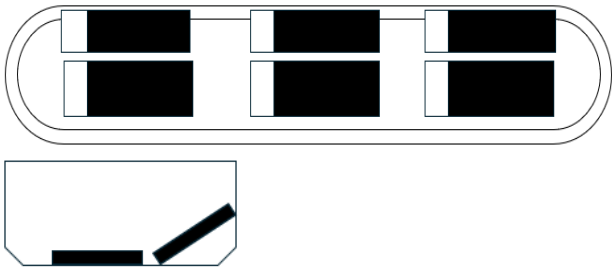

Figure 2-4: Simplified layout of 3D foams in the ceramic boat. Top: top-down view from right to left 1M, 0.5M, 0.25M samples 1 and 2. Left: cross section view demonstrating angled foam sample position.

2.3.2 Analysis of SEM images for concentration variations

SEM analysis of these samples was used to assess uniformity of coating, and thickness. Figure 2-3 to the left shows the 1M PAN solution substrates. As the first look at the substrates with polymer on it seemed as if it was going to be very convenient with how clear and easy it was to identify the polymer and thickness. The dark metal substrate stands out easily and the cPAN illuminates brightly (because the polymer is not as conductive as the metal substrate). The bright color of the cPAN is likely from a buildup of charge in locations that are sufficiently separated from the nickel. In the previous experiments this study was built around Dr. Windsor identified that while conducting cPAN itself will store charge and acta as a conductor[7]. In these images the polymer maintaining the shape of the substrate and a noticeable gap because of the well-preserved shape of the polymer despite delamination from the substrate suggests that the separation comes from difference in shrinking during the nitrogen freezing and cutting. A significant and even coating should hold material in place even when fractured. During battery cycling the cell shouldn't be exposed to a cold enough environment cause this delamination. Centered in image A there is an example of this, a bright cPAN strip has separated from the nickel exposing a lighter colored bare nickel. At the separation point there is darkened, still well adhered, cPAN. The charge from the electron beam is still dissipated sufficiently with the thickness of this layer but when contact is not close the charge does build up slightly as it cannot ground instantly to the metal. When nonconductive material has

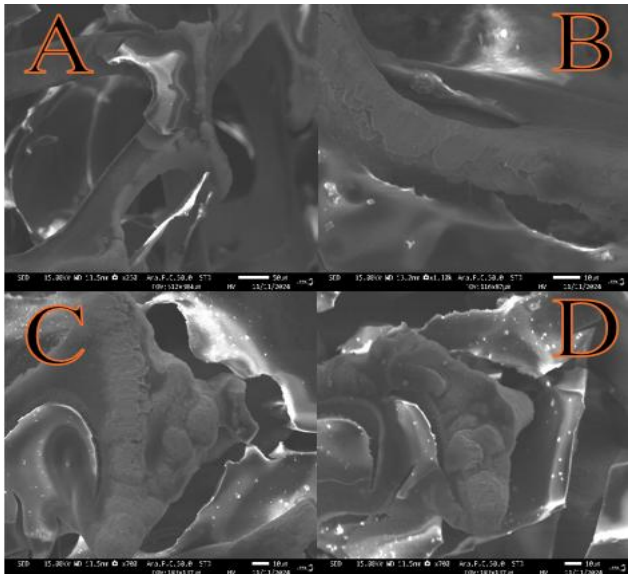

Figure 2-5: SEM images of cPAN from 1M PAN solution. TOP- A/B PAN 1 sample. Bottom- C/D PAN 2 sample.

been observed in the past it has been blurry, and the full material was as bright as the some of the edges in particularly in Figure 2-5 images C and D. The average thickness of this material is consistent and around 250 nm.

In Figure 2-6 observations are made on the substrates that were dipped in the 0.5M PAN solution. On these samples there were numerous small points where charge accumulates, in G and H these occur at the end of clumps of cPAN as they end up too far separated from the substrate. This suggests that this more dilute solution results in a thinner polymer that can adhere better to the substrate, particularly during extreme temperature changes such as the nitrogen freezing. However, there was more inconsistency with the textures and thickness through this material. Images G and H coming from 0.5 M PAN 2 and being the sample that was annealed at a slight angle have very thin flaky layers that span between 100-150 nm. The 0.5 M PAN 1 sample was less flaky with smooth layers that were mostly also in the 100-150 nm range but included the pocket seen in F where the layer was around 1 µm.

Figure 2-6: SEM images of cPAN from 0.5M PAN solution. TOP- E/F PAN 1 sample. Bottom- G/H PAN 2 sample.

Figure 2-7 shows 0.25 M PAN 1 and 2 samples also resulted in thin and flaky polymer layers. Many of these layers were very thin and difficult to determine thickness as edge surfaces while attached to the substrate were difficult to identify and those that were separated are thin and not typically in plane to measure. Most estimates are 50-100 nm. In every image there were missing

chunks and fractures or missing PAN material not at or near the cut surface. The much thinner material has the advantage of being more flexible, like in the 0.5M solution, but seems to be mechanically weaker and less resilient resulting in polymer loss. Since the desire was for a resilient polymer layer, the 1M solution was used for future work, to avoid the potential of flaky material associated with the 0.25M and 0.5M solutions.

Figure 2-7: SEM images of cPAN from 0.25M PAN solution. TOP- I/J PAN 1 sample. Bottom- K/L PAN 2 sample

2.3.3 SEM analysis with dipping variations

Looking at the consistency vertically, when observing the number of dips changing in hindsight likely should have been repeated under the same conditions as when changing the concentration, i.e. everything should have been cut horizontally or everything cut vertically. Additionally, in many of these images the substrate seemed crushed but there was little delamination external to the struts of the substrate. Figure 2-8 to the right shows a variation external coating is often even, with a few thick spots. In all 3 parts of Figure 2-8 there are charged cPAN portions internally. This caused a review of the previous samples that indicated this was also present at lesser extents in the 1M and 0.5M samples. M is an image taken from the bottom of the sample dipped 25 times, N the middle of sample dipped 50 times, and O the top of the sample dipped 100 times. The thickness of these cPAN layers were in the 200-300 nm range across all samples. This would suggest that after additional dips after 10

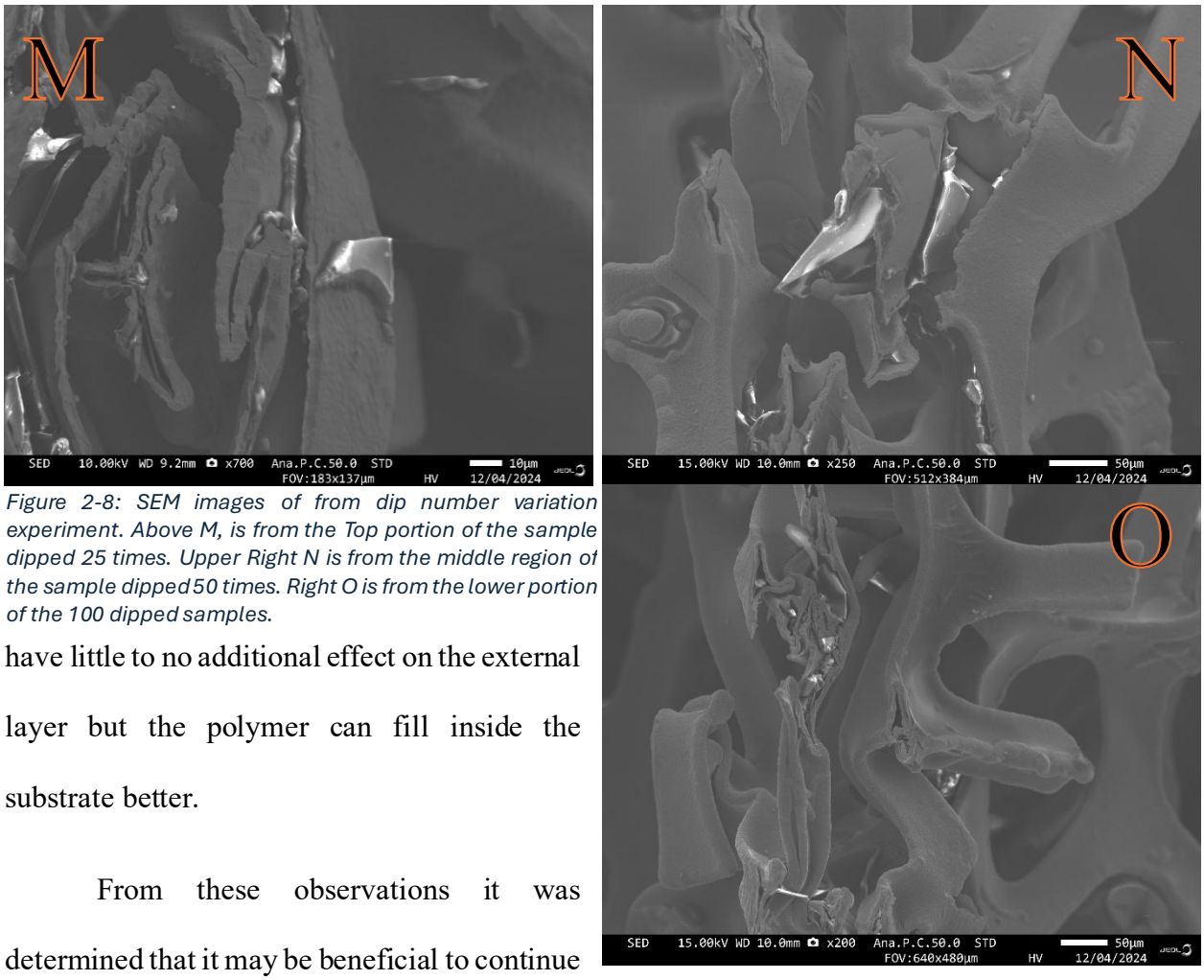

Figure 2-8: SEM images of from dip number variation experiment. Above M, is from the Top portion of the sample dipped 25 times. Upper Right N is from the middle region of the sample dipped 50 times. Right O is from the lower portion of the 100 dipped samples.

have little to no additional effect on the external layer but the polymer can fill inside the substrate better.

From these observations it was determined that it may be beneficial to continue to dip all substrates 25 times in the 1M solution to try allowing polymer to fill and seal the edges to minimize electrolyte filling internally to the substrate. However, currently it is uncertain whether this extra polymer on the inside of the struts contributes or hinders the cells' operations in any meaningful way. This would be an interesting area of research for anyone picking up this project in the future.

2.4 References

(1) (PDF) Intrinsic Thermodynamic and Kinetic Properties of Sb Electrodes for Li-Ion and Na-Ion Batteries: Experiment and Theory. *ResearchGate* **2025**. https://doi.org/10.1039/C3TA11568B.

(2) Lee, S. High Energy All-Solid-State Li-Ion Batteries.

(3) Li, X.; Wu, D.; Luo, Q.; An, J.; Yin, R.; Wang, D. Advanced Cyclized Polyacrylonitrile (CPAN)/CdS Nanocomposites for Highly Efficient Visible-Light Photocatalysis. *J. Mater. Sci.* **2017**, *52* (2), 736–748. https://doi.org/10.1007/s10853-016-0367-9.

(4) Zhang, W.; Sun, M.; Yin, J.; Abou-Hamad, E.; Schwingenschlögl, U.; Costa, P. M. F. J.; Alshareef, H. N. A Cyclized Polyacrylonitrile Anode for Alkali Metal Ion Batteries. *Angew. Chem. Int. Ed.* **2021**, *60* (3), 1355–1363. https://doi.org/10.1002/anie.202011484.

(5) Leroy', S.; Boiziau, C.; Perreau, J.; Reyxaud, C.; Zalczer, G.; LkAYOW', G.; Ix, C. _MOLECZTLAR STRUCTHRF OF KN ELECT-ROPBLYMERIED.

(6) *Table 1 Major IR bands in the spectra of PAN fibers*. ResearchGate. https://www.researchgate.net/figure/Major-IR-bands-in-the-spectra-of-PAN-fibers_tbl1_284693868 (accessed 2025-03-04).

(7) *Multifunctional Cyclized Polyacrylonitrile (cPAN) as a Coating for Sb-Based Anodes in Sodium-Ion Batteries | ACS Applied Materials & Interfaces*. https://pubs.acs.org/doi/full/10.1021/acsami.4c13887?casa_token=Zu3rrmH6K7AAAAA%3AUnNh035jMIYlw7PpkP9KcJAVpicnSuX7l3b_qUR8MUEIrZZPQ-p5_haGBwADczmcVYBy7WlbNomI (accessed 2025-03-19).

Chapter 3- Fabrication of Pouch Half-Cells to study the Effects of cPAN on Anodes for Sodium-ion Batteries

3.1 Background

Studying a battery comes the major challenge of having a variety of distinct components that need to be individually optimized for their characteristics but optimized collectively for their effects on each other. It is impossible to study one component of a battery without assembling it into a device where its properties may be convoluted by the properties of the other components. In theory there is an uncountable number of materials that can work as an anode and each would need to be studied for its best effects, what becomes practical as a useful anode will become limited when considering the cathode material, and vice versa. In many of today's lithium-ion batteries, the anode consists of graphite, silicon, or a mixture of the two. These materials can be complimented by a condensed list of cathodes including lithium iron phosphate ($LiFePO_4$, LFP), lithium nickel manganese cobalt oxide ($LiNi_xMn_yCo_zO_2$, NMC), or lithium cobalt oxide ($LiCoO_2$) cathodes[1,2]. However, when one of the materials changes the other may no longer complement the new component. This challenge is more acute when considering a transition from lithium to sodium. The primary anodes used for lithium-ion batteries, graphite and silicon, do not sodiate, and hence are not viable candidates for anodes in sodium ion batteries.

When a full cell battery is operating, the overall trends and how well the battery is doing are important. However, to study how individual components work separately from each other, a half cell can be constructed to observe how those components operate (where the material of interest is cycled versus sodium metal as a reference)[3]. In my undergraduate research, led by Dr.

Nieto, various electrolytes were examined for their effects against a consistent anode in a half cell[4]. Out of this set of experiments the electrolyte that performed best for the antimony anode was used in the experiments described in this dissertation. Dr. Nieto was also capable of making an operable 3D battery using similar conditions ,which would be used as the control for this experiment with one notable exception. The sodium used in her experiments was a solid 1 cubic cm cube and was required to be calendared, expending a large number of hexanes for safety. Because equipment for this experiment is in various locations this meant transporting the sodium in containers through the public and flattening the sodium outside of an air free environment adding additional risk and potential cross contamination with the projects at the second site. To mitigate the risks associated with direct reproduction and repeating this process, a composite sodium foil roll was purchased. The sodium on this foil was flat but adhered to an aluminum current collector using an unidentified polymer, shown above in Figure 3-1.

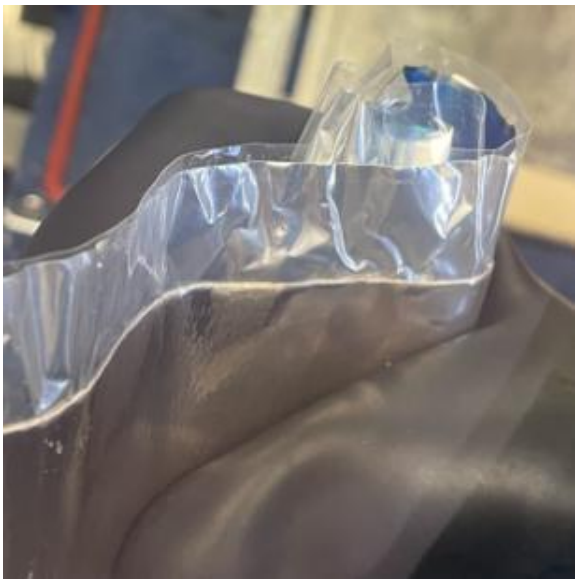

Figure 3-1: Close image of the composite sodium material. The grey material closet in the forefront of the image is the sodium, and shiny silver material in the back is the aluminum current collector. Between the two is a white material serving as a binder, that is unidentified from by manufacturer.

3.2 Experimental

3.2.1 Solution preparation and verification.

For consistent active material through this experiment, every deposition solution was made in the same manner, in either 100 ml or 200 ml volumes. These solutions consisted of 200 mM

sodium gluconate or D-gluconic acid sodium salt (Sigma-Alrich, >98%), 30 mM of (1-hexadecyl) trimethylammonium bromide (CTAB) (Alfa Aesar, >99%), and 30 mM of antimony (III) chloride (Sigma-Aldrich,). Millipore water was used as a solvent and the mixture was heated to 60℃ while stirring for an hour to ensure everything was fully dissolved. Since there are variations in day-to-day conditions (such as the temperature in the lab), to ensure the proper potential is used when depositing the solutions are analyzed prior to electrodeposition via cyclic voltammetry (CV) on a Gamry Instruments Reference 3000 potentiostat (GIR 3000). The reduction and oxidation peaks of the solution were verified over three cycles scanned in the range of potential from 1.25 V to -1.25 V at a scan rate of 50 mV/second verse a silver/ silver chloride electrode (Ag^+/AgCl).

3.2.2 Anode Cleaning, Deposition and Observations

As with chapter 2, a 1 cm x 4 cm x 1.25 mm nickel foam substrate was used. The mass of the substrate was measured and a 1 cm x 1 cm area at the end of one side was compressed with an accessible flat metal, such as a ruler or metal plate left at the workstation to give a flattened surface for future steps. To ensure cleanliness of the nickel and remove the surface oxide layer, the substrate was sonicated in an isopropyl alcohol (IPA) solution for three minutes. It was then rinsed with IPA and quickly dried by placing under a stream of air to remove excess liquids in a process referred to as being quick-dried. It was then placed in 5M hydrochloric acid (HCl) and sonicated for three additional minutes. The substrate was then rinsed with DI water, IPA, and ethanol, quick-dried again and placed in solution for deposition.

The substrate was connected as the working electrode with the 3 cm uncompressed portions submerged, and with two 6 cm x 8 cm stainless steel fine mesh sheets, which were each folded in half and used as counter electrodes, each about 2 cm away from the working electrode. The same Ag^+/AgCl reference was used parallel to the substrate between the counter electrodes. Using the

GIR 3000 a repeating chronoamperometry experiment was run without stirring using the potential of the primary reduction peak identified in the CV for 10 seconds, then rested at 0 V verses open circuit potential for 15 seconds to allow for diffusion to replenish chemicals lost to deposition around and internally to the foam. This was repeated for sixty cycles. The sample was then removed from solution and rinsed with DI water, IPA, and ethanol, before being quick-dried and weighed for deposited mass.

Typically, a 100 ml solution can make three to four samples before there is a significant drop in material deposited, so the samples all deposited in the same day were either designated control or experimental. Samples in the control group were expected to behave similarly to what was seen by Dr. Nieto. The experimental group was coated in cPAN using the procedure determined through chapter 2. Each sample was observed on a JOEL JSM-IT800 by SEM, and energy dispersive X-ray spectroscopy (EDS), to observe material patterns and consistency of layers.

3.2.3 Electrolyte preparation

Electrolytes for the cells are made in an argon glovebox. This consists of 1M sodium perchlorate ($NaClO_4$) in polyethylene carbonate (PC) with 5% fluoroethylene carbonate (FEC). The electrolyte was allowed to mix for at least 12 hours prior to transferring to a separate glovebox for cell fabrication.

3.2.4 Half-Cell pouch construction and operation

Fabrication of the pouch cells takes place off campus at Prieto Battery, an exploded view diagram of a pouch cell is provided in Figure 3-2. A nickel tab (B) for the current collection is added to the anode (C) with a Sonics and Materials, Inc. MW20SC sonic welder. The exposed

bare nickel is covered in a nonreactive high-temperature lithium battery terminal tape (MTI) to prevent incidental contact and shorting. The substrate is loosely double wrapped in a Beyond Battery celgard 2500 microporous polypropylene membrane sleeve (E) to serve as a mechanical separator. A second 1.5 cm x 7 cm current collector is cut from a textured copper roll and is also given a tab (D). Two separate 1.5-inch x 2.5-inch sheets are cut from an aluminum foil to make the actual pouch (A), having 2 sides, one shiny and one dull. The shiny side has a polyamide layer on polyester-polyurethane that when heated above 180-190 °C will melt to form an airtight seal. The dull side is coated with polypropylene. Once all these parts are prepped, the first seal for the half cells is made using an MTI MSK-140 Hot Sealing Machine, with the seal about 1 cm from the top edge of the pouch along the meltable adhesive on the tabs (G). The first few millimeters of the top edge are cut and folded over and covered with terminal tape. The extended tabs should be bent in a controlled manner to prevent contact and shorting the cell in future steps. At this point there should be an anode protected by polypropylene separator and texture side of the current collector facing it, on one side of the pouch cell sealed.

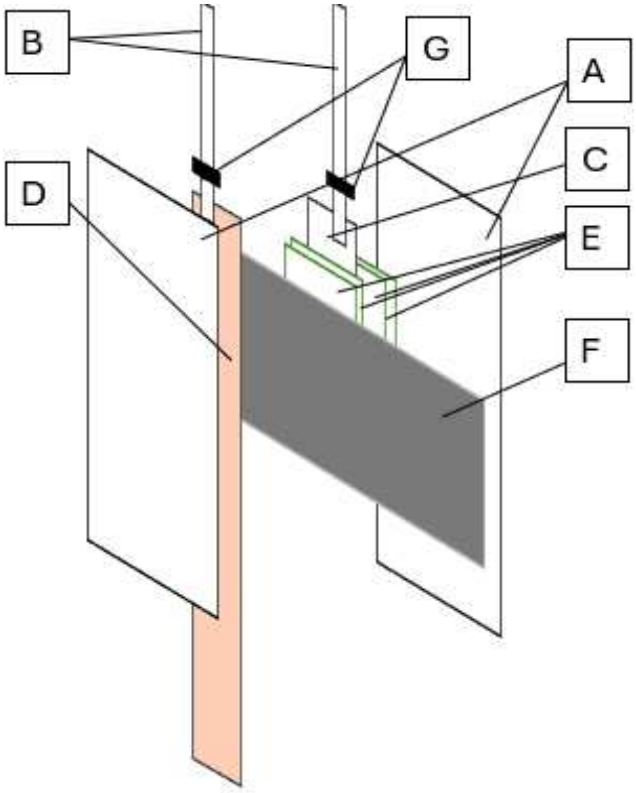

Figure 3-2: Exploded view diagram of a pouch half-cell. A- coated material to make pouch. B- Nickel tabs. C- Anode. D- Copper current collector. E- Polypropylene pouches, this is not 4 small sheets but 2 sealed pouches that covers the full substrate with an opening at the top. F- Sodium cathode material. G- Adhesive material for sealing tabs in the pouch

This assembly is then pumped into an argon glovebox, and a 3 cm x 3 cm sheet of composite sodium foil (MTI, >99.7%) is cut to wrap around the anode. This sheet is cleaned of oxide layers by gently brushing it with a soft bristled toothbrush before wrapping around the anode ensuring there is slight overlap at the ends. The copper current collector is then also wrapped over the sodium material, and the side and the bottom of the pouch are sealed using an MTI MSK-115A Vacuum Sealing Machine. Finally, 1.2 ml of electrolyte is pipetted into the pouch and placed into an MTI MSK-170 Vacuum Standing Box (diffusor). The diffusor draws a -60 kPa vacuum for 15 seconds, equalizes to 0, then draws a -80 kPa vacuum for 14 seconds before equalizing to 0, and repeats both vacuum steps for a total of 4 flushes of the chamber to ensure all trapped gases in the electrolyte are removed. The last side of the pouch is sealed in the vacuum sealer under a -72 kPa vacuum.

After removal from the glovebox and returned to campus, each cell was checked via a voltmeter to ensure shorting did not occur in transit. After approximately 12 hours each cell resistance was checked via electrochemical impedance spectroscopy (EIS) in the GIR 3000. They were then placed on an Arbin battery cycler to cycle under a schedule that would check internal resistance against the theoretical capacity and attempt 500 charge/ discharge cycles, from 2 V to 0 V.

3.3 Results and Discussion

3.3.1. Pre-deposition Verifications.

Antimony alone in water would readily oxidize quickly to form various oxides. The primary purpose of the sodium gluconate is to ensure that the antimony stays in the 3+ state for deposition. Given variations in day-to-day conditions some shifts in potential for the reduction of antimony may occur. Despite small variations day to day, in general a CV such as Figure 3-3 is expected with the primary peak around -1V vs Ag^{+}/AgCl, most of the batteries were deposited using -1.05 V for a given amount of time. By maintaining this potential over an extended period of time the antimony can reduce from the 3+ state and form solid antimony on the surface of the electrode.

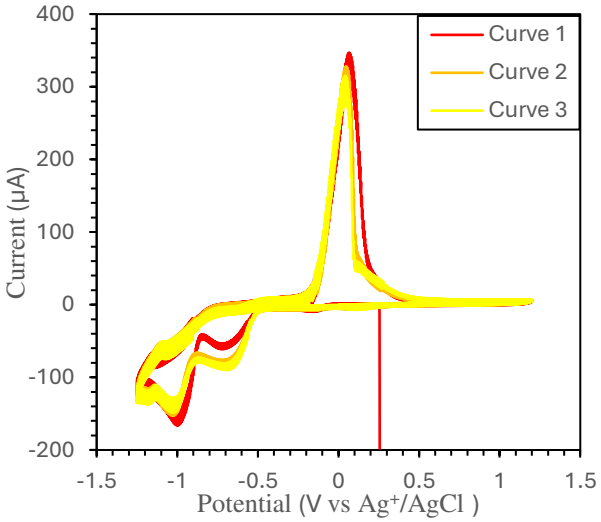

Figure 3-3: Typical CV for an antimony solution for 3 cycles vs. an Ag^{+}/AgCl reference electrode. Key points to observe are the reduction peaks at -1V and -0.7V, as well as oxidation peak around 0.1V.

3.3.2 Observations of the Deposited Substrates.

The polymer demonstrated the same level of resilience and ability to maintain its shape as seen in chapter 2, but interestingly during the freezing process the cPAN formed crystalline patterns such as those observed in Figure 3-4, circled in green. An EDS image of the patterns showed no extra interesting patterns or special structures of the polymer and since the freezing conditions that made the patterns weren't in the scope of the experiment it wasn't investigated further. One site showing separation of the cPAN to observe what kind of layers were left underneath was seen near the upper portions of the foam. Figure 3-5 shows this delamination where there is little distortion on the surface of the polymer (region in red), though small amounts of material are visible on the surface of the substrate (with a few larger deposits circled in blue). This

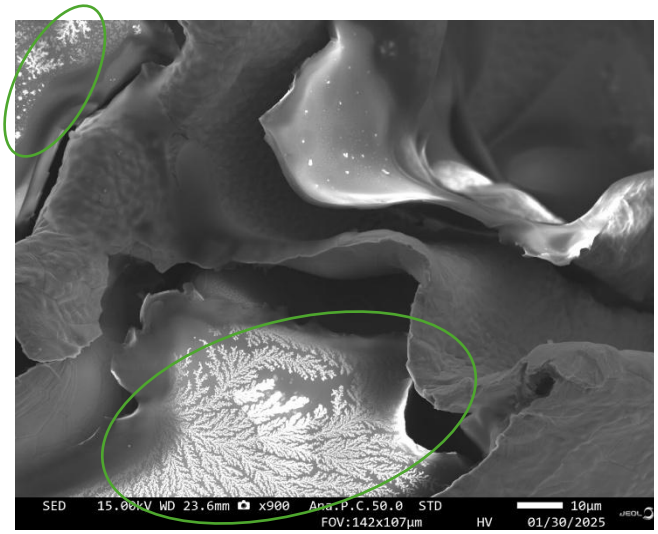

Figure 3-4: SEM image of cPAN coated externally and internally on the strut of the nickel foam. Unlike previous samples periodic crystalline deposits, circled in green were seen in the polymer.

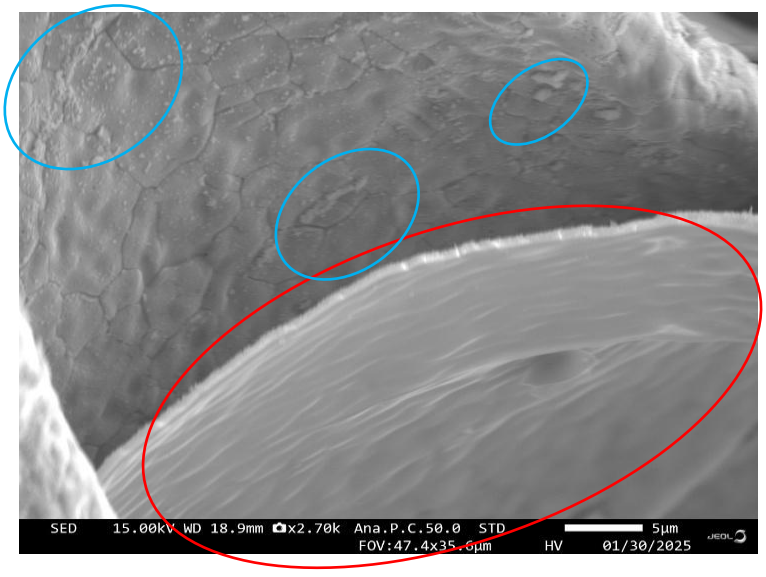

Figure 3-5: SEM image of cPAN layer delaminating from the substrate to reveal trace amounts of antimony deposits. Surface of the polymer to observe is circled in red, and key antimony on the substrates are circled in blue. The patterns of these deposits are not transferred to the surface of the polymer.

showed that there could be material mass masked by the layers of the cPAN. At the time it was a concern that the polymer may be too thick for sodiation to occur. Nearby was the point of a strut that was cut that didn't expose the inside. EDS was used for Figure 3-6 to help discern the differences in the nickel and cPAN layers. In the layered composite the carbon and nitrogen elements are nearly indistinguishable from each other due to the high dispersion of nitrogen in the polymer. Despite the layers of the cPAN there is sufficient antimony detection over all parts of the nickel substrate, except for the charged section of cPAN in the lower right corner.

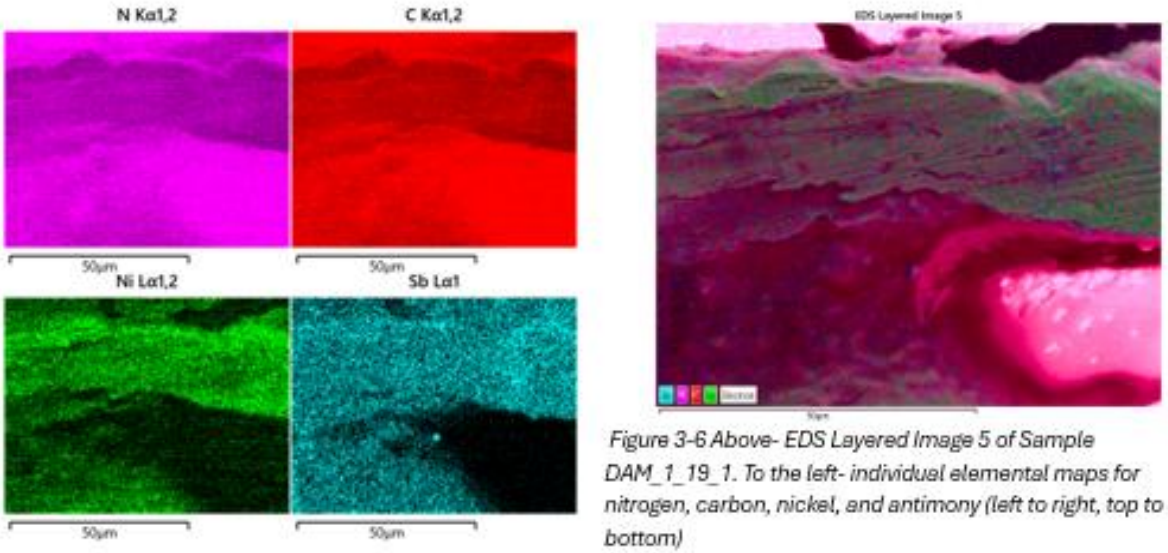

Figure 3-6 Above- EDS Layered Image 5 of Sample DAM_1_19_1. To the left- individual elemental maps for nitrogen, carbon, nickel, and antimony (left to right, top to bottom)

As discussed in chapter 1, outer edges near points tend to experience more dendritic growth and valleys often see less deposition, these areas were also a focus for observation. To the right Figure 3-7 shows dendritic growth of antimony (in blue) on a point in Layered Image 1, and minimal antimony available in valleys in layered image 2. Much like in Figure 3-5, the cPAN coating (crimson combination of red carbon and purple nitrogen) stays flat and together, while anything that sticks up from the current collector too much is no longer covered. Since the core concept of the hypothesis is that the polymer will keep the material in contact when it fractures

and separates at the base and as visible in the middle of layered image 1 of Figure 3-7, with a bright yellow arrow, there is polymer in between some of the sections of the material as it extends, this will help test the hypothesis. These images of Figure 3-7 also demonstrate that there is material exposed and accessible for sodiation; because of this the previous concerns of the polymer thickness issues were temporarily satisfied, and it was determined it should be fine moving forward and making these batteries. Additionally, of the six EDS scans on this sample, the four with antimony protruding through the cPAN layer each had trace amounts of oxygen over almost every part of the sample. The two without protruding antimony had no oxygen detected. Though undesired, unexpected delays between the liquid nitrogen freezing and cleaving step, and subsequent SEM/EDS scans resulted in the anode being exposed to air, likely resulting in the formation of antimony oxides. Because this sample was frozen and cut, and would not be used in a cell, along with regions without exposed oxide detected it was not considered, our hypothesis is that presence of oxides will not impact the characterization of polymer coating and thickness.

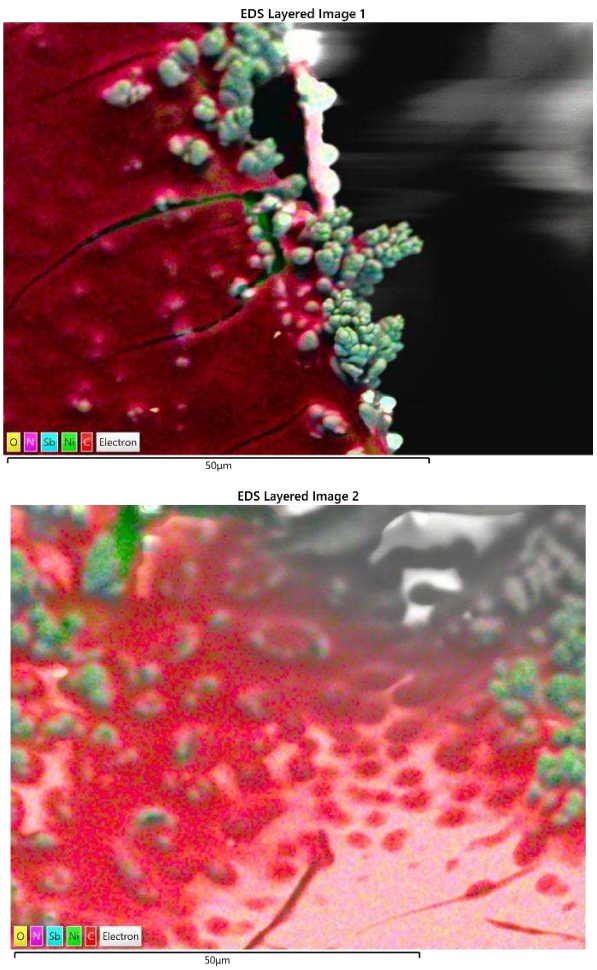

Figure 3-7: Top- EDS Layered Image 1 dendritic growth of antimony particles, from struts on the outer edge of a point. Bottom- EDS Layered Image 2 valley between struts with minimal antimony in blue on the bottom and sufficient deposited antimony to not be fully covered on the walls approaching a point. Both imaged from DAM_1_19_1

3.3.3 Resistance evaluation

EIS data in Figure 3-8 shows for the samples without cPAN there are 2 significant electronic events occurring in the cell in which the various parts of the cell may be acting as two sets of parallel resistors and capacitors[5]. These plots are meant to observe the real and imaginary impedance of the cell, which allows the system to be modeled like a circuit and mathematically fit to determine what the values may be. When the real impedance is at the higher end of the curve, data flattens into a line with a slope that deviates from the theoretical 45 degrees expected for a Nyquist plot but can be the end tail that can be used to determine the Warburg impedance, a factor that reflects mass transfer considering linear diffusion. The middle region has a semi-circle reflective of one set of a capacitor and resistor in parallel. At the lower end of the real resistance the imaginary resistance climbs for samples DAM_1_17A and C. This is indicative of the set in the series. However, the frequencies associated with these events are above the limit of what the available potentiostat can do, and the full set associated with it is important for proper analysis of the data. Sample DAM_1_17_B seems to be a representative set of data for this evaluation, further exploration into what the various shifts and curves in the tail mean for a Warburg impedance are underway. For determining the resistance that the components are collectively providing to the cell an internal resistance check step was implemented into the Arbin

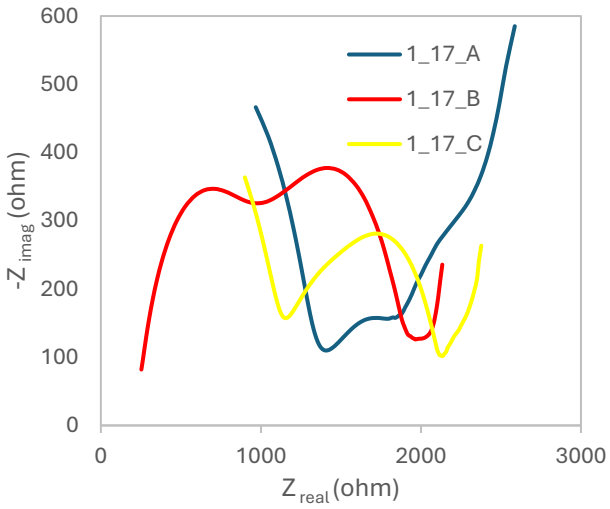

Figure 3-8: Nyquist plots from EIS surveys scanned from 1 MHz-100 mHz. DAM_01_17_A (blue), Z_{real} ranges from 700-2550 ohms, $-Z_{imag}$ ranges from 100-700 ohms. DAM_1_17_B (red) Z_{real} ranges from 250-2150 ohms, $-Z_{imag}$ ranges from 80-390 ohms. DAM_1_17_C (yellow) Z_{real} ranges from 900-2400 ohms, $-Z_{imag}$ ranges from 150-400 ohms.

cycling schedules to help determine the identify patterns or issues associated with the cells. After issues with getting the cells to cycle at normal rates, alligator clips were placed on the cells to apply pressure and help maintain contact to the current collector, and they were cycled at a rate of C/10.

The same process was repeated with the cPAN cells. The issues with the incomplete data set persist, but the curves maintain very distinct shapes. The second semi-circle exists in these curves but to a much lesser extent, suggesting that the circuit is the same with significantly different values. The composite sodium sheet around DAM_1_19_4 was cut smaller than desired and to ensure the anode was completely surrounded a second small strip was cut. The best way to complete contact was to have the sodium sides of the strips both facing the anode and making contact to each other on the sides. Because of this DAM_1_19_4, bottom of Figure 3-9, was then expected to have a different trend in shape when compared to the other two. Due to the higher resistance issues these cells require a rate of C/50 to properly cycle.

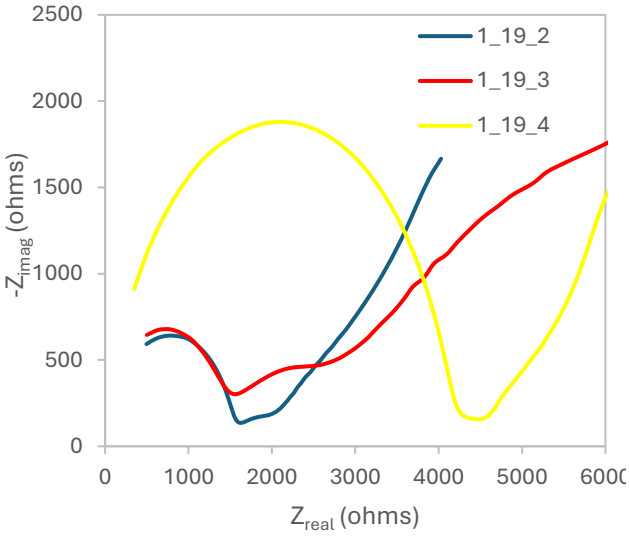

Figure 3-9: Nyquist plots from EIS surveys scanned from 1 MHz-100 mHz. DAM_01_19_2 (blue) Z_{real} ranges from 250-4050 ohms, $-Z_{imag}$ ranges from 100-1800 ohms. DAM_1_19_3 (red) Z_{real} ranges from 500-7000 ohms, $-Z_{imag}$ ranges from 200-2000 ohms. DAM_1_19_4 (yellow) Z_{real} ranges from 300-5750 ohms, $-Z_{imag}$ ranges from 150-1600ohms.

The resistance of the cells obtained from the internal resistance check written into the schedule file once cycling is listed in Table 3-1. When comparing the uncoated anodes these seem to be consistent, though the EIS curves had no consistency in shape. Despite a range within the cells, they fall within a 50 Ω window. However, the resistance variability of the cPAN coated cells shows there is significantly less predictability. These resistances in DAM_1_19_2/3/4 also show that wrapping the composite sodium material around the anode as a single longer strip is preferred over the 2 shorter but still in contact used in DAM_1_19_4.

Table 3-1: Arbin schedule run internal resistances for each of the cells. As determined by a check run at the start of the 300-cycle run at C/10 or C/50 when clamped.

Cell ID (DAM_1_XX_X)	Resistance (Ω)
17_A	280
17_B	271
17_C	320
19_2	3792
19_3	1355
19_4	4095

3.3.4 Evaluation of Cycling Data

When initially placed on the Arbin battery cycler and attempting a C/10 schedule all batteries immediately failed. Further review of the available data at the time showed with all of the resistances so high the currents of the intended schedule caused the voltage limit of the step to be exceeded immediately, and the next step to start but suffer the same problem, following Ohms Law (equation 1). This resulted in the cells "finishing" hundreds of charge/ discharge cycles in a few minutes.

$$Equation\ 1: V = IR$$

V: Voltage, I: Current, R: Resistance

This led to obtaining basic data cycle rates of C/100 for the uncoated samples, and samples that were coated were unable to collect data. Various methods were used to attempt to get the cells at a more normal rate, including placing them all under several large books to get even weight distribution, but only clamping them with alligator clips were successful as mentioned in the resistance portion. Cells DAM_1_17_B and C failed shortly into the clamped cycling, most likely due to excessive handling and damage to the mechanical separator causing a short, and to be investigated during cell disassembly. Final comparable data for the half-cells will be to the half-cell sample DAM_1_17_A.

Figure 3-10 shows the specific capacity of the uncoated half-cell when cycled without the alligator clip. In the first cycle of the cell low efficiency is expected due to an initial stored charge of these cells typically around 2.7V. In anode study half-cell conditions are typically reversed from what they would be in a full cell, so a discharge cycle in a half-cell is when a negative potential is applied to the prepared anode (acting as the cathode) and the prepared anode is sodiated, when a charge step is applied then a positive potential is applied and the anode desodiates. In a normal full cell, a negative charge applied to the prepared anode acting as the anode still sodiates it but is the charge step. The coulombic efficiency in the first few cycles may jump as the material fully sodiates and the SEI forms. Changes in specific capacity indicate inaccessible or lost material that is no longer participating in charge transfer. As previously

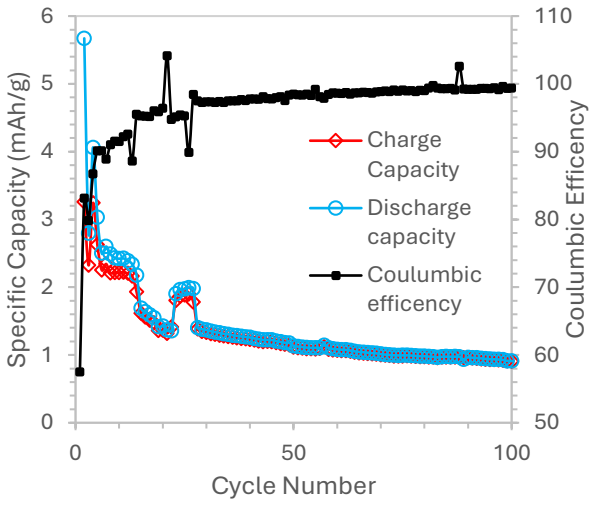

Figure 3-10: Cycling data forDAM_1_17_A early life, unclamped, at a rate of C/100, truncated at the range of 100 cycles to help spread data out.

mentioned, antimony has a specific capacity of 660 mAh/g. Figure 3-10 shows that DAM_1_17_A unclamped had just shy of 6 mAh/g available when first put on the cycler, and after about 75 cycles had fallen to less than 1 mAh/g. This stabilizes to around 0.75 mAh/g and goes the full 500 cycles planned with little extra anomalies. There is an unexpected trend around cycle 12 in which the specific capacity drops and returns to a similar capacity around 22, then drops again to return to the same capacity trend it was on in the previous drop just before 30. These cycles would be several days apart, and jumps are likely due to the cell shifting and either material separating or reconnecting while troubleshooting was occurring to the Arbin cycler swapping cells in the tower.

After being clamped and cycled there is a was a drastic return in specific capacity in Figure 3-11. Despite being less than 1 mAh/g in the previous attempts, in the first cycle there was a jump to 15 mAh/g and an upward trend for several cycles after that, hitting a discharge specific capacity peak of 417 mAh/g and a charge specific capacity peak of 386 mAh/g. Final specific capacities come to around 70 mAh/g at 95 cycles. This cell was stopped early to process data. This demonstrates the importance of contact between the anode and current collector. If there isn't sufficient contact with the current collector then regardless of contact of the anode, separator, and cathode within the system charge transfer cannot occur. This trends closer to what would have been expected for this cell, a high specific capacity that decays around 50 cycles.

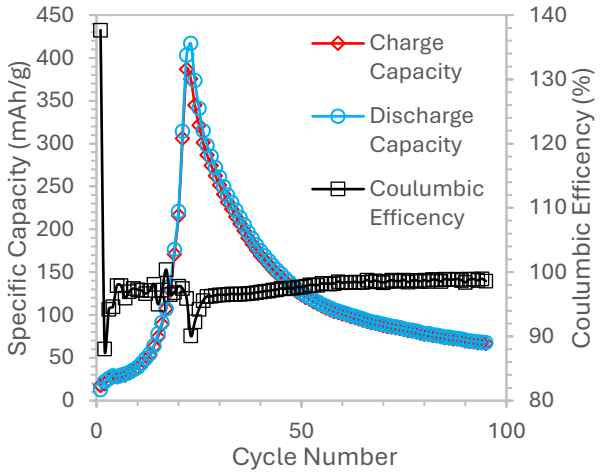

Figure 3-11: Cycling data forDAM_1_17_A after adding an alligator clip, at a rate of C/10. Interesting peaks occur around 20 cycles. 95 complete cycles.

Figure 3-12 is the first view at cycling data for a cPAN coated anode. There is a large drop in capacity right in the first cycle. Again, this was expected though more than desired. There are abnormal cycles that occur at 13 and 16 though nothing stands out more than maybe some extra movement of the battery when something else may have been added or removed from an adjacent space. The holding bracket is not designed to maintain pouch cells, so they see more movement than a normal cell during cycling. Figure 3-13 provides a different and unexpected look for cell data. Much like in Figure 3-12 there is a sharp drop in capacity in the first cycle and following a decay the specific capacity settles out. The core difference in these cells is after 50 or so cycles the cell show some recovery and begins to gain capacity. Closer observation of Figure3-12 shows a slight and slow uptick in capacities. If more time had been allowed it may have been possible for DAM_1_19_3 to also reach 55-60 cycles and potentially begin to show a large increase in capacity. While sudden capacity loss is typically indicative of material loss or inaccessible material, capacity gain is less precedented. However, the logic should follow that rapid material loss represents rapid capacity loss, rapid capacity gain should mean rapid material gain. Since it is impossible for us to place additional material into the cell once fabricated this suggests that the material is slowly then rapidly made accessible again within the cell.

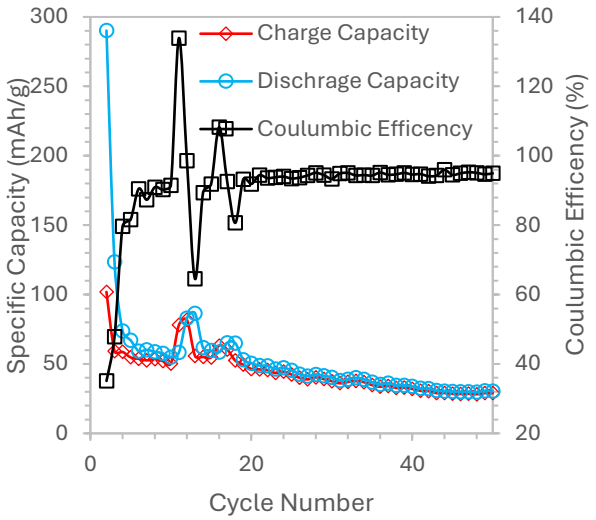

Figure 3-12: Specific capacity for DAM_1_19_3 with alligator clip, at a rate of C/50. Key cycles are around 13 and 16. 49 complete cycles.

These three clamped cells were placed on the cycler within 20 minutes of each other. The various actual mass on each sample shifted the expected capacity, and as such the C-rates. Since the actual capacity associated with each sample wasn't exact, the time spent cycling also wasn't as exact, resulting in significantly different cycles completed for each sample. With just about 3 weeks cycling, at the scheduled rates DAM_1_17_A should have only finished 25 cycles and DAM_1_19_2/3 would have completed 5. As the specific capacities show, there is considerably less material accessible than calculated, the amount available over time changes noticeably for each cell. For the cells containing cPAN this loss in the beginning cycles and eventual return can be explained revisiting work out of our lab by Dr. Windsor and discussed in chapter 2. Not only does cPAN hold charge but it has the ability to hold and retain sodium itself[6,7]. The low initial capacity is likely due to the cPAN inhibiting sodium access to a majority of the active material, but the delay in which cycle the capacity returns is reflective of how long it takes for the sufficient sodium to move through the thick cPAN layer and interact with the covered antimony.

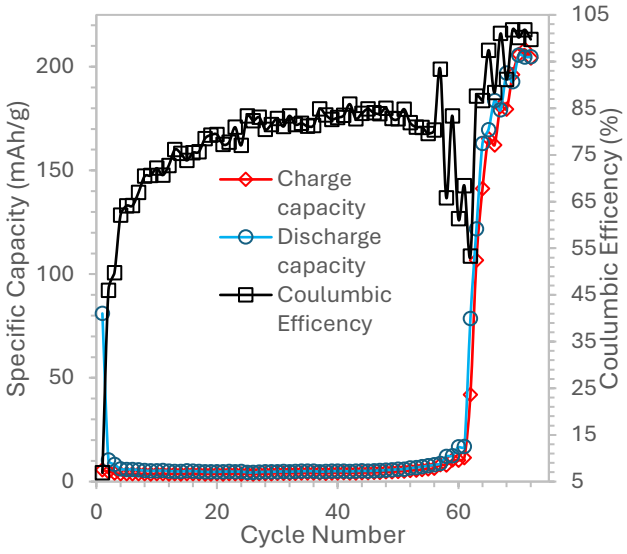

Figure 3-13 Specific capacity data for DAM_1_19_2 while clamped, at a C/50 rate. 72 complete cycles.

3.4 References

(1) Chen, M.; Liu, Q.; Wang, S.-W.; Wang, E.; Guo, X.; Chou, S.-L. High-Abundance and Low-Cost Metal-Based Cathode Materials for Sodium-Ion Batteries: Problems, Progress, and Key Technologies. *Adv. Energy Mater.* **2019**, *9* (14), 1803609. https://doi.org/10.1002/aenm.201803609.

(2) Fang, C.; Huang, Y.; Zhang, W.; Han, J.; Deng, Z.; Cao, Y.; Yang, H. Routes to High Energy Cathodes of Sodium-Ion Batteries. *Adv. Energy Mater.* **2016**, *6* (5), 1501727. https://doi.org/10.1002/aenm.201501727.

(3) *Half-Cell Battery: What It Is And Its Role In Electrochemical Energy Storage [Updated On-2025]*. https://poweringautos.com/what-is-a-half-cell-battery/ (accessed 2025-03-12).

(4) Nieto, K. Tuning Antimony Anodes Through Electrodeposition to Inform on the Reaction and Degradation Mechanisms in Sodium Ion Batteries, Ph.D. Dissertation, Colorado State University, 2023.

(5) Lazanas, A. Ch.; Prodromidis, M. I. Electrochemical Impedance Spectroscopy─A Tutorial. *ACS Meas. Sci. Au* **2023**, *3* (3), 162–193. https://doi.org/10.1021/acsmeasuresciau.2c00070.

(6) Windsor, D. S.; Perez, M. J.; Snyder, E. R.; Neisius, N. A.; Otten, R. A.; Hall, S. C.; Tibbetts, C. A.; Krummel, A. T.; Prieto, A. L. Multifunctional Cyclized Polyacrylonitrile (cPAN) as a Coating for Sb-Based Anodes in Sodium-Ion Batteries. *ACS Appl. Mater. Interfaces* **2025**, *17* (1), 2117–2129. https://doi.org/10.1021/acsami.4c13887.

(7) Zhang, W.; Sun, M.; Yin, J.; Abou-Hamad, E.; Schwingenschlögl, U.; Costa, P. M. F. J.; Alshareef, H. N. A Cyclized Polyacrylonitrile Anode for Alkali Metal Ion Batteries. *Angew. Chem. Int. Ed.* **2021**, *60* (3), 1355–1363. https://doi.org/10.1002/anie.202011484.

Chapter 4- Integrating a cPAN anode into a Full Cell

4.1 Background

As mentioned in chapter 3, half-cells are vital to deconvolute some of the data happening in a full cell so that a specific electrode can be studied. But ultimately a battery must contain both an anode and a cathode to operate with high energy density and longevity. Consequently, if something is tested to improve either an anode or a cathode it will ultimately need to be tested in a full cell to see if it can work in those conditions as well. Due to time constraints these batteries had to be fabricated and placed on the Arbin battery cycler prior to full collecting data for the half cells. Since at the time there were difficulties getting proper operations of the batteries, it was difficult to predict trends or anticipate how these cells should react. While no conclusive evidence has been collected that cPAN will enable longer cycle life for antimony on a 3D current collector, this chapter provides compelling initial results that the approach for coating 3D electrodes is viable.

4.2 Experimental

Anodes were deposited under the same conditions as for the half-cells in chapter 3. Sodium chromium oxide ($NaCrO_2$) laminates were prepared with the assistance of the cathode development team from Prieto Battery Inc. The cathode laminates were prepared via planetary mixing in a Kurabo Mazerustar (KK-250S 100V) and then sheet cast on 15µm Al foil using an Automatic Film Applicator (TQC Sheen 1133N). They were then dried at 120°C under vacuum. The sheets of cathode material were then cut to size with an Epilog Fusion Pro (17000) laser cutter and the tab area was cleaned with IPA. Each laminate was calendared to 30% porosity using a

Felix Calendaring Machine (FM-JS250). Under normal conditions the mass of active material for the anodes and cathodes would be made to in capacity (the N to P ratio). However, since the cathode laminates were already made and would otherwise be wasted, a batch of anodes were made to roughly match the existing cathode laminate capacities.

The fabrication of a full cell is done similarly to the half cells detailed in chapter 3. Figure 4-1 highlights these differences. Instead of using the current copper collector, the pair of cathode laminates are connected using a short aluminum strip which is sonically welded to an aluminum tab (B/E/F). Since a piece of solid sodium was not required the top, bottom, and one of the sides can be sealed using the heat-sealing machine. Inside the glove box 1.2 mL of the same electrolyte used in chapter 3 was used and after being diffused the final side was sealed in the vacuum sealing machine.

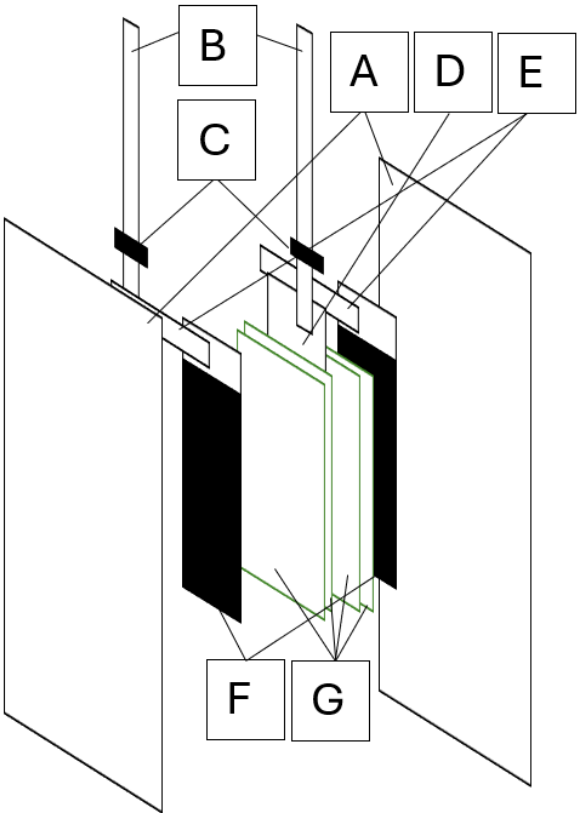

Figure 4-1: *Exploded view diagram of a full cell pouch. A- coated material to make pouch. B- Nicke/Aluminum tabs. C- Adhesive material for sealing tabs in the pouch D- Anode E-Extender for cathode tabs. F- Cathode. G- Polypropylene pouches, this is not 4 small sheets but 2 sealed pouches that covers the full substrate with an opening at the top.*

After being allowed to rest the full cells for roughly 12 hours, all cells were connected to the GRI 3000 for EIS surveys ranging from 3 kHz to 100mHz. They were then all attached via alligator clips and placed on the Arbin battery cycler. Each full cell was then given a

schedule that checked internal resistance, charged to 4.0 V, discharged to 2.6 V (both at a C/50 rate), and set to repeat the charge /discharge phase 301 times.

4.3 Results and Discussion

4.3.1 Abnormalities in Fabrication of the Full Cells

With nearly thirty cathode laminates to choose from, in pairs for one on each side of the anode, ten anode depositions were made attempting to target the desired matching capacity. This resulted in four anode capacities that were too high, three were too low and could only be matched with a single laminate, and three were capable of matching a pair of laminates that matched within about .1 mAh. Pairs were matched and six cells were planned. To get an even distribution within the six cells, three were made without cPAN, two having two capacity matching cathode laminates, and one would only have one laminate with equivalent capacity. Conversely three were coated with cPAN and split to have one with two capacity matching laminates and two with only one laminate that matched in capacity.

The cathode laminate tabs were required to be changed to aluminum because the energy required to weld the nickel tabs to the laminate base is too high and would tear the base and the cathode material would break off. The energy for the aluminum tabs is enough to cause damage to the active material if it is too close to it and weakens the base making it brittle and breakable if overly worked or handled. This happened when trying to weld the tab to the connector of anode DAM_1_21_A4, a cPAN coated anode, the base broke and the cell had to be scrapped. While this was one of the paired capacity matched samples, having two laminates each about half the value of the anode, a cathode with equivalent capacity to the anode alone was not available. The Anode

*Table 4-:1 Anode and cathode matching data. Anode IDs come from 10 substrates weighed out in a grid pattern to track masses. Cathode laminate A/B/C come from a variation in laminate thickness. A:15 mil, B:20mil, and C:25 mil. With mil being thousands of an inch. *Prepped but broken cathode resulting in lost cell.*

Anode ID (DAM_01_21_XX)	*Anode Capacity(mAh)*	*cPAN Dips*	*Laminate ID (N110P151_XX)*	*Cathode Capacity(mAh)*
A2	2.7	25	B8	2.7
A3	5.9	25	B2/B3	3.3/2.7
*A4**	13.6	25	C2/C3	6.9/6.3*
C1	3.7	-	B12	3.5
C2	3.1	-	B10	3.0
B1	4.6	-	A7/A8	2.4/2.2

IDs, capacity, if they had a cPAN layer, and the laminate cathode IDs with their capacities are detailed in Table 4-1. These are very small anodes at 4 cm x 1 cm and a 1 cm x 1 cm working area to attach a tab to. A partnered cathode should be the same size but with a smaller tab area of about 1 cm x 0.5 cm. The surface area of the region of contact on the sonic welder is about 1 cm x 2 cm. This means there is little room for errors and leaving an error tolerance gap to ensure that the welder is not too close to the material that the vibrational energy breaks the material alone gives even less room to work with. The large number of cathode laminates is to ensure sufficient pairs because breakage is common with these materials. Ultimately with no shorts, five of six cells making it to being placed on the battery cycler on the first attempt for a new process is a high yield rate.

4.3.2. Full-Cell analysis data

The general layout of the full cells is an interior anode with material, a mechanical separator, then cathode. After the cell starts to operate and SEI layer forms that will also play a role. The modeled circuit for this is to the right in Figure 4-2A[1]. However, with the loose mechanical separators used in the pouch cells, the path of least resistance, figuratively and literally, for the electrolyte is around the separator and not through it. For these reasons, the full cells should look like the half cells modeled in Figure 4-2B[1], maybe with an additional semi-circle feature. DAM_1_21_B1 and C2 are both shown in Figure 4-3, both show what looks like an extra semi-circle feature. Extending the EIS scan an extra two decades to 1 mHz and overlaying the curves on top of one another the general shapes are maintained. DAM_1_21_C2 with the lowest combined resistance has the easiest time identifying

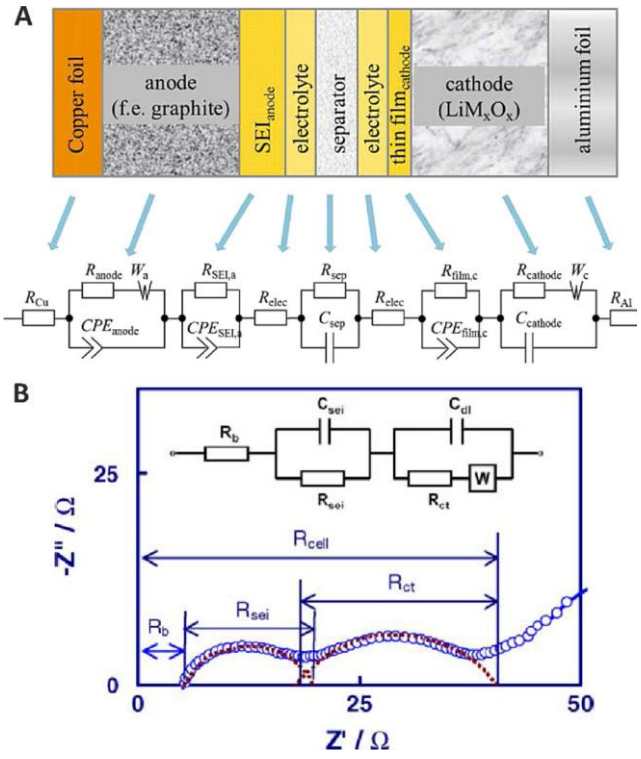

Figure 4-2: (A) individual cell components described as equivalent circuit elements, for a full cell. (B) Circuit model equivalent for a Lithium-ion Half-Cell. Taken from Lazanas. A. and Prodromidis, M. figure 27.

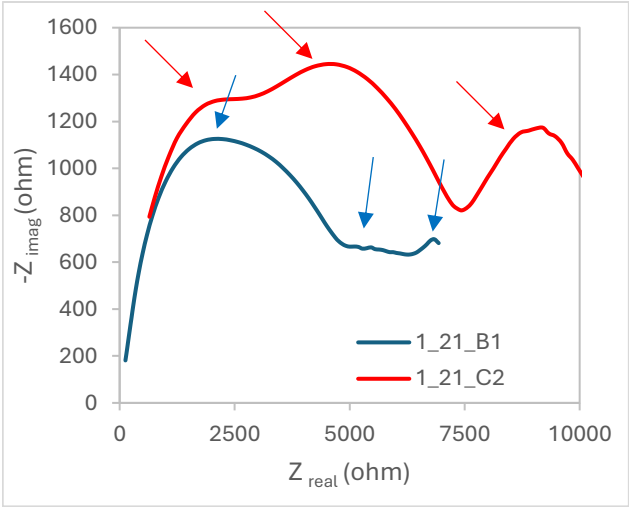

Figure 4-3: Nyquist plots from EIS 300KHz-100mHz. DAM_1_21_B1 (blue). Bottom- DAM_1_21_C2 (red). Arrows are used to assist in identifying the "peaks" in identifying semicircle shapes.

all three peaks. Where DAM_1_21_B1 is only a little more resistive and 2 of the peak's blends with the tail. The other three each had two semi-circle components suggesting at least one of the events is masked by the resistance of the other two.

Once on the Arbin with alligator clips clamping the cells, the first resistance step obtained the data featured in Table 4-2. There is a significant amount of resistance. Though the rate was slow, the first charge operation worked almost as expected and all cells reached the desired 4.0V, though between two and three hours. However, at this point all cells experienced large spikes in voltage during transitions from charge to discharge. This caused step end conditions to trigger, and all cells finished the desired 301 cycles in around 10 minutes, for a total test time on average of three and a half hours. This means how the cPAN coating affects the full cell environment could not accurately be evaluated.

Table 4-2 Cell resistance data from Arbin resistance step, identified by the Anode in cell.

Anode ID (DAM_1_21_XX)	Arbin Resistance (Ω)
A2	5174
A3	11273
C1	5430
C2	4427
B1	4249

4.4 Conclusions and Future Works.

4.4.1 Full Evaluations and Criticisms

Through every step of this experiment, internal resistance created significant problems. While in a research environment it is possible to slow down rates to observe reactions and to verify if what we expect to happen occurs, in any commercial application this is not reasonable. Most cells of this size do not operate at μA/h rates. Despite that there were interesting results at the end of chapter 3 showing recovery of cells containing cPAN and maintained pressure between the

electrodes. This suggests that if resistance issues can be resolved, cPAN can have a future in supplementing anodes to extend lifetime.

Each chapter of this dissertation was built on the results of chapter 2 and the full cells had to be started prior to completion of half-cell cycling for time. This means that while each section can have core ideas learned, full evaluation of the processes cannot be considered without all parts together. While many of the resistance issues experienced in chapter 3 were expected to have been from the change from sodium metal to the composite sodium electrode material, a review of Dr. Nieto's thesis never indicated the resistance of that cell[2], and it had a significantly higher amount of material from a much more aggressive deposition. Because a significant resistance issue persists when moving to a full cell, a few other possibilities are considered. With personal experience in industry, substrates are typically calendared or compressed prior to deposition to reduce diffusion path lengths lowering resistance barriers, as cPAN itself will increase the diffusion coefficient of the sodium[3]. Additionally, from the high resistance issues encountered in the full cell experiments of chapter 4, we can also conclude that the composite sodium is less likely to be the direct issue for resistance. Throughout this experiment concentrations were low with very soft deposition parameters. A more aggressive deposition with increased active material available, though a larger substrate will be required, as cathode slurries and thicknesses can be limited on size.

We believe a critical error was made in the basis of the experiments in chapter 2. The 1M solution was chosen because it produced cPAN films with a reasonable thickness and lack of flakiness so that it would maintain its shape when the active material expanded and contracted. In the second part of the experiment the number of dips varied, resulting in slightly thicker layers. The use of a lower concentration of PAN should have been pursued and more dips in the 50+ range could have made it more resistant to cracking or flaking. The use of a 0.5M PAN solution with

more than 10 dips could create a cPAN layer in the 150-200 nm range, to reduce the diffusion path through the polymer and strengthen the layer as mentioned above. A thinner polymer layer is less likely to block electrolyte paths further into the substrate, which can be shorter but narrower when calendared due to an increased tendril density.

4.4.2 Next steps

Future experiments should be focused on the use of the 0.25M PAN solution when coating the anode. In the 1M solution there was negligible additional mass added when going from fifty to one hundred dips so it will likely be less than fifty required for the desired thickness. Calendaring may also prove to be useful, reducing the diffusion pathlength to the material in the center of the substrate significantly depending on the calendared thickness. Finally, something to distribute the pressure maintained more than along the mm thick edge of the alligator clips may also prove to be useful, though would be the lowest priority. Although EIS surveys of the cells should also include some form of added pressure contact with current collectors is key to getting the full scope of useful and reliable data. From this data set alone one could not confidently state for certain that cPAN can extend the life of a cell by maintaining active material in electrical contact to the substrate. But following this experiment and reviewing lessons learned up to this point, we should remain hopeful that it is possible on a 3D substrate.

4.5 References

(1)Lazanas, A. Ch.; Prodromidis, M. I. Electrochemical Impedance Spectroscopy─A Tutorial. *ACS Meas. Sci. Au* **2023**, *3* (3), 162–193. https://doi.org/10.1021/acsmeasuresciau.2c00070.

(2) Nieto, K. Tuning Antimony Anodes Through Electrodeposition to Inform on the Reaction and Degradation Mechanisms in Sodium Ion Batteries, Ph.D. Dissertation, Colorado State University, 2023.

(3) Windsor, D. S.; Perez, M. J.; Snyder, E. R.; Neisius, N. A.; Otten, R. A.; Hall, S. C.; Tibbetts, C. A.; Krummel, A. T.; Prieto, A. L. Multifunctional Cyclized Polyacrylonitrile (cPAN) as

a Coating for Sb-Based Anodes in Sodium-Ion Batteries. *ACS Appl. Mater. Interfaces* **2025**, *17* (1), 2117–2129. https://doi.org/10.1021/acsami.4c13887.